THE JOURNAL OF PHYSICAL CHEMISTRY A
A JOURNAL OF THE AMERICAN CHEMICAL SOCIETY

pubs.acs.org/JPCA Article

Molecular Properties of Thorium Hydrides: Electron Affinities and Thermochemistry

Monica Vasiliu, Mary Marshall, Zhaoguo Zhu, Kit H. Bowen,* and David A. Dixon*

Cite This: J. Phys. Chem. A 2022, 126, 2388−2396 Read Online

ACCESS | Metrics & More | Article Recommendations | Supporting Information

ABSTRACT: High-level electronic structure calculations of the ground and low-lying energy electronic states for ThH_x and ThH_x^- for x = 2−5 are reported and compared to available anion photoelectron detachment experiments. The adiabatic electron affinities (EAs) are predicted to be 0.82, 0.88, 0.51, and 2.36 eV for x = 2 to 5, respectively, at the Feller−Peterson−Dixon (FPD) level. The vertical detachment energies (VDEs) are predicted to be 0.84, 0.88, 0.81, and 4.38 eV for x = 2−5, respectively. The corresponding experimental VDEs are 0.871 eV for x = 2, 0.88 eV for x = 3, and 4.09 eV for x = 5. As for ThH, there is a significant spin−orbit (SO) correction for the EA of ThH_2, and this correction decreases substantially for x > 2. The observed ThH_2^- photoelectron spectrum has many transitions as predicted at the CASPT2-SO level. The FPD bond dissociation energies (BDEs) increase from 67 to 75 kcal/mol for x = 2 to x = 4 at the FPD level. The BDE for ThH_5 is much lower as it is a complex of H_2 with ThH_3. The hydride affinities for x = 2 to 4 are all comparable and near 70 kcal/mol. A natural bond orbital analysis is consistent with a significant Th^+-H^- ionic contribution to the Th−H bonds. There is very little participation of the 5f orbitals in the bonding and the valence electrons on the Th are dominated by 7s and 6d for the neutrals and anions except for ThH_2^- where there is a significant contribution from the 7p.

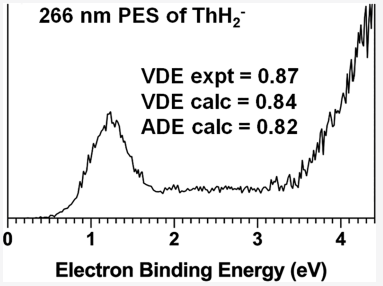

INTRODUCTION

Thorium is an early member of the actinide series with chemistry that often exhibits transition metal-like chemistry. A number of experiments have been reported on small molecular anions containing Th. The experimental electron affinity (EA)[1] of Th obtained using photoelectron spectroscopy (PES) is 0.607690(60) eV. A calculation[1] at the multiconfigurational Dirac Hartree−Fock level with a large basis set is consistent with this value. Other calculated EAs for Th are consistent with this value including 0.59 eV [CCSD(T)/CBS limit using aug-cc-pwCVnZ basis sets plus an effective core potential for Th][2] and 0.565 eV [beyond the CCSD(T) level including an all-electron four-component relativistic treatment of spin−orbit (SO)].[3] The EA of ThH arises from a complicated PES spectrum and has been calculated at the Feller−Peterson−Dixon (FPD) level[4−7] using a combination of CCSD(T)/CBS calculations with additional higher order correlation and relativistic corrections, and SO corrections at the MRCI level to be 0.82 eV.[8] Using a combination of PES and correlated molecular orbital theory, ThH_5^- was shown to be a superhalogen molecule with a vertical detachment energy (VDE) of 4.09 eV.[9] These authors also briefly described results for ThH_3^-.

Andrews and co-workers[10] reacted Th atoms with H_2, D_2, HD, and H_2/D_2 gas mixtures to produce ThH_xD_y neutrals in the Ar and Ne matrices. The experimental vibrational frequency for ThH in a Ne matrix is 1511.0 cm^{-1}, consistent with the CCSD(T)/awQ-DK values for ν(ThH $^2\Pi$) of 1530 cm^{-1} and ν(ThH $^2\Delta$) of 1537 cm^{-1}.[8] For ThH, the $^2\Pi$ state is the ground state at the CCSD(T) level and the $^2\Delta$ state is the ground state at the CASPT2 + SO level. Grant et al.[11] have reported neutron diffraction and computational results on much larger Th−H complexes with a variety of ligands.

In the current work, we use a combination of PES experiments and high-level correlated molecular orbital theory calculations with SO corrections to investigate the structures (geometries and vibrational frequencies) and electronic and energetic properties of neutral and anionic $ThH_x^{-/0}$ molecules for x = 2−5. The new PES data are for ThH_2^- and the data for ThH_3^- and ThH_5^- are taken from prior work.[9]

EXPERIMENTAL AND COMPUTATIONAL METHODS

Experimental Section. The ThH_2^- anions were produced and analyzed using a house-built anion photoelectron spectrometer, which has been described in detail previously.[12] The apparatus consists of an ion source, a time-of-flight mass spectrometer, a Nd/YAG photodetachment laser, and a magnetic bottle energy analyzer. The thorium dihydride anions were generated in a laser vaporization ion source. A rotating,

Received: March 1, 2022
Revised: March 25, 2022
Published: April 12, 2022

https://doi.org/10.1021/acs.jpca.2c01460
J. Phys. Chem. A 2022, 126, 2388−2396

translating thorium rod was ablated using the second harmonic of an Nd: YAG laser (532 nm, 2.33 eV), while 20 PSI of UHP H_2 gas expanded over the Th rod. After pulsing H_2 gas over the rod for a minute, the gas flow was shut off, and the experiments were conducted using no backing gas. The resulting anions were then extracted before entering the photodetachment region.

Anion PES experiments were conducted by crossing the mass-selected anion beam with a fixed-energy photon beam and energy analyzing the resulting photodetached electrons. The photodetachment process is governed by the energy conservation relationship, $h\nu$ = EBE + EKE, where $h\nu$ is the photon energy, EBE is the electron binding energy, and EKE is the electron kinetic energy. The second (532 nm, 2.33 eV) and fourth (266 nm, 4.66 eV) harmonics of a Nd/YAG laser were used to photodetach the ThH_2^- anion. The photoelectron spectra were calibrated against the known transitions of Cu^-.[13] The resolution of the magnetic bottle energy analyzer is ~50 meV at 1 eV EKE.

Computational Methods. Building on our computational approach for the prediction of the electronic affinity and ionization potential of ThH,[8] two sets of calculations were performed. One set used the composite FPD approach to obtain a quantitative prediction of the EAs. The other set used the complete active space self-consistent field (CASSCF) method together with second-order perturbation theory (CASPT2) and SO coupling via the state interacting approach to predict the low-lying excited states of the neutrals and anions. Both are described in detail below.

The geometries were optimized and the harmonic frequencies of ThH_2, ThH_3, ThH_4, and ThH_5 and the corresponding anions were calculated at the CCSD(T)[14−17] (coupled cluster theory with single and double excitations with a perturbative triples correction) level with the third-order Douglas−Kroll−Hess Hamiltonian (DKH3).[18−20] The aug-cc-pV*n*Z-DK for H[21,22] and the cc-pwCV*n*Z-DK3 for Th[23,24] for n = D and T basis sets were used for the geometry and frequency calculations; these are denoted as aw*n*-DK. These calculations included the correlation of the valence electrons (H 1s, Th 6s, 6p, 6d, and 7s) and the Th 5s, 5p, and 5d core−shell electrons. In addition, single-point calculations were performed at the awQ-DK level on the awT-DK geometries, and in some cases, the geometries were optimized at the awQ-DK level. The CCSD(T) total energies were extrapolated to the CBS limit by fitting to a mixed Gaussian/exponential (eq 1)[25]

$$E(n) = E_{CBS} + A\exp[-(n-1)] + B\exp[-(n-1)^2] \quad (1)$$

with n = D through Q (n = 2, 3, and 4). Equation 1 was chosen as it works best for extrapolation to obtain dissociation energies using the D, T, and Q basis sets.[26] The open-shell calculations were performed using the R/UCCSD(T) approach where a restricted open-shell Hartree−Fock calculation was initially performed and the spin constraint was then relaxed in the coupled cluster calculation.[27−30] The CCSD(T) calculations were performed using the MOLPRO program package.[31,32] The calculations were performed on our local University of Alabama Opteron- and Xeon-based Linux clusters.

To obtain SO corrections for all the ThH_x species (neutral and anion for x = 2, 3, and 4), state-averaged CASSCF[33,34] calculations were performed to represent the lowest states, using the aug-cc-pV*n*Z basis sets[35,36] for H and the cc-pV*n*Z-PP basis sets with effective core potentials for Th,[23,37] for n = D, T, and Q. These basis sets are noted as a*n*-PP. To choose the orbitals for correlation, an ionic model is used where the H^- anion is treated as a closed shell. Thus, ThH_2 gives Th(II) for which the low-lying states correspond to singlets and triplets from the low-lying $5f^16d^1$ and $6d^2$ atomic ion configurations.[38] ThH_2^- gives Th(I) for which the low-lying states correspond to doublets and quartets from the $6d^17s^2$ atomic ion configuration. For ThH_2, the CASSCF(2/8) has two electrons in eight orbitals, with all of the lower energy orbitals constrained to be doubly occupied. The CASSCF(3/8) active space for ThH_2^- includes three electrons in the same effective eight orbitals. The CASSCF for ThH_3 with Th(III) results in doublet states arising from a single valence electron on the metal in eight orbitals. ThH_3^- gives Th(II) again, so there are singlets and triplets arising from the two electrons in eight orbitals. The choice of eight orbitals is based on our work[8] on ThH and that of others[39−41] on ThX, where X is a halogen. This choice is based on the anionic nature of the ligands and the need to incorporate the active orbitals on the Th, which are the 7s, 6d, and selected 7p.

Post-CASSCF calculations using the same active spaces as the preceding CASSCF calculations were carried out via second-order perturbation theory (CASPT2).[42,43] Multiple states are calculated using a Fock operator constructed from a state-averaged density matrix and the zeroth-order Hamiltonians for all the states. The frozen-core definition in the CASPT2 included all the orbitals of Th through the 5d (6s6p5f7s valence). The smallest possible IPEA shift[44] was used, a value of 0.28 for all the states.

The state-interacting method for the treatment of SO coupling,[45] implemented in MOLPRO, was used to calculate the molecular states at the SO-CASPT2 level. The SO eigenstates are obtained by diagonalizing H_{el} + H_{SO} based on H_{el} eigenstates. The matrix elements of H_{SO} were constructed using the SO operator from the Th pseudopotential. Here, the SO matrix elements have been calculated throughout at the CASSCF level of the theory, with the diagonal terms of H_{el} + H_{SO} replaced with CASPT2 energies. These calculations were performed using the a*n*-PP basis set at the corresponding optimized aw*n*-DK bond distances for n = D, T, and Q.

This combined approach yielded an EA of 0.764 eV for ThH as compared to a value of 0.820 eV when full T and Q corrections at the CCSD level were included (0.029 eV), a KRCI/MRCI calculation for the SO (0.016 eV), and a QED correction for the Lamb shift (0.011 eV) where the values in parentheses are the additional missing values.[8]

To obtain a better understanding of the bonding for these neutral and anionic ThH_x species, the Natural Population Analysis results based on the natural bond orbitals (NBOs)[46,47] using NBO7[48,49] are calculated using the MOLPRO program package at the aD-DK level.

RESULTS

The mass spectrum of the anions produced when laser ablating a Th rod in the presence of H_2 is presented in Figure 1. ThH_x^- anions were produced, where x = 0, 1, and 2. The PES spectra collected from photodetaching the ThH_2^- anions using the second (532 nm, 2.33 eV) and fourth (266 nm, 4.66 eV) harmonics of a Nd/YAG laser are presented in Figure 2a,b, respectively. The fourth harmonic produces a PES spectrum with one broad peak with an onset of 0.571 eV and maxima of 1.239 eV. The second harmonic PES spectrum highlights the

https://doi.org/10.1021/acs.jpca.2c01460
J. Phys. Chem. A 2022, 126, 2388−2396

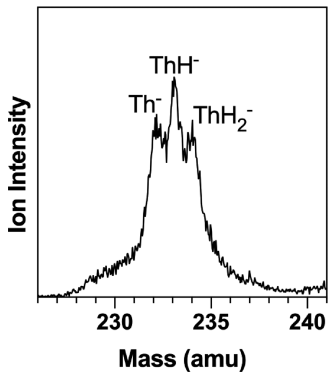

Figure 1. Mass spectrum obtained by laser ablating a Th rod in the presence of H_2.

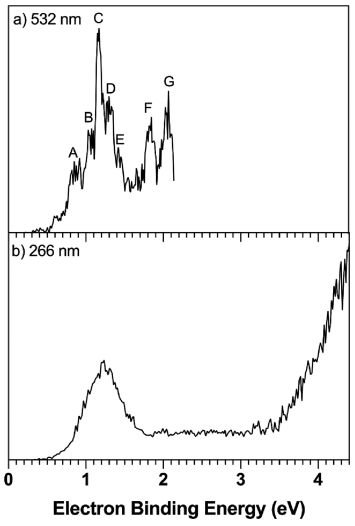

Figure 2. PES spectra of ThH_2^- collected using the (a) second harmonic (532 nm = 2.33 eV) and (b) fourth harmonic (266 nm = 4.66 eV) of a Nd/YAG laser.

many transitions between the ThH_2 anion and neutral. There are seven dominant photodetachment peaks. The extrapolated peak maxima are listed in Table 1.

Table 1. Extrapolated Peak Maxima for the PES Spectra of ThH_2^-[a]

peak	EBE maxima (eV)
A	0.871
B	1.054
C	1.199
D	1.333
E	1.458
F	1.895
G	2.119

[a]Collected using the second harmonic of a Nd/YAG laser (532 nm = 2.33 eV). The error bars on the peaks are ±0.013 eV.

Molecular Geometries. The molecular geometry parameters are given in Table 2. ThH_2 and ThH_2^- are bent with C_{2v} structures. The bond angle in the neutral is 6° smaller than in the anion, and both bond angles are greater than 125°. The bond distance increases in the anion from that in the neutral by 0.09 Å. The ground state of ThH_2 is $^1A_1$, and the first excited

Table 2. Calculated Geometry Parameters for $ThH_x^{0/-}$ (x = 1−5) at the CCSD(T)/awT-DK Level[a]

$ThH_x^{0/-}$	symmetry	spin State	ΔE_{0K}[b] kcal/mol	r(Th−H) Å	∠(H−Th−H)°
ThH	$C_{\infty v}$	$^2\Pi$	0.0	2.008	
ThH	$C_{\infty v}$	$^2\Delta$	0.2	2.023	
ThH^-	$C_{\infty v}$	$^3\Phi$	0.0	2.108	
ThH_2	C_{2v}	$^1A_1$	0.0	2.036	125.1
ThH_2	C_{2v}	$^3B_1$	6.6	2.066	117.1
ThH_2^-	C_{2v}	$^2B_1$	0.0	2.126	131.3
ThH_2^-	C_{2v}	$^2A_1$	0.03	2.126	131.2
ThH_3	C_{3v}	$^2A_1$		2.073	116.3
ThH_3^-	D_{3h}	$^1A_1'$	0	2.121	120
ThH_3^-	C_s	$^3A''$	9.0	2.173	119.8(x2)
				2.152(x2)	107.5
$^1ThH_4$	T_d	$^1A_1$		2.079	109.5
$^2ThH_4^-$	D_{2d}	$^2A_1$		2.166	128.4(x2)
					100.9(x4)
$^2ThH_5$	C_s	$^2A'$		2.082(x2)	112.6
				2.073	112.3(x2)
				0.792 (H−H)	
$^1ThH_5^-$	C_{4v}	$^1A_1$		2.186(ax)	133.6 ax eq
				2.154(eq)	81.1 eq eq
$^1ThH_5^-$	D_{3h}	$^1A_1'$	3.0(2i)[c]	2.144 eq	120
				2.239 ax	90

[a]Values for ThH and ThH^- from ref 8 and are given for comparison purposes. [b]Relative energies at the CBS/awn-DK level. [c]Not a minima, two large imaginary frequencies (see text).

state is a $^3B_1$ state, which is 6.6 kcal/mol higher energy. There is a second excited $^1A_1$ state 7.8 kcal/mol above the ground state with a small bond angle and a $^3A_1$ 8.0 kcal/mol higher in energy than the ground state. The electronic structure of the anion is somewhat more complicated as there are two very low-lying doublet states, $^2B_1$ and $^2A_1$, that are essentially isoenergetic, with the $^2A_2$ state only 3.4 kcal/mol above the ground state. This will be discussed in more detail below.

ThH_3 is a trigonal pyramidal, a $^2A_1$ state with C_{3v} symmetry, and the anion is a planar $^1A_1'$ state with D_{3h} symmetry. The vertex inversion barrier in ThH_3 is only 0.4 kcal/mol (CBS/awn-DK), so that the molecule is very similar to ThH_3^- except for the bond distance. The bond distance in ThH_3 increases by 0.04 Å from that in ThH_2. The bond distance in ThH_3^- increases by 0.05 Å as compared to ThH_3 and is slightly smaller than the Th−H bond distance in ThH_2^-.

ThH_4 is a tetrahedral $^1A_1$ state with no active Th electrons in the ionic model. The bond distance in ThH_4 is very similar to that in ThH_3. The addition of an electron to form the ThH_4^- anion leads to a distortion from T_d symmetry to D_{2d} symmetry, generating a $^2A_1$ state. The bond distance in ThH_4^- increases by 0.09 Å from that in the neutral.

The structures for ThH_5 and ThH_5^- have been previously reported, and our optimized structures are in agreement with the prior reported structures.[9] ThH_5^- has a C_{4v} symmetry ($^1A_1$) with Th−H bond distances similar to those in ThH_4^-. This anionic ThH_5^- structure differs from the trigonal bipyramidal, D_{3h}, structure predicted for ThF_5^-.[50] The D_{3h} structure for ThH_5^- has a degenerate imaginary frequency of 293i at the aD-PP level and is 3.0 kcal/mol higher in energy. The structure of ThH_5 is asymmetric with the H_2 complexed to a ThH_3 in C_s symmetry but canted off to one side. The H_2

https://doi.org/10.1021/acs.jpca.2c01460
J. Phys. Chem. A 2022, 126, 2388−2396

bond distance is 0.05 Å greater than that of the isolated H_2 diatomic (0.743 Å) at this level of theory. This differs significantly from the $ThF_3^+F_2^-$ ion pair structure predicted for ThF_5.[50] The H_2 is bound to the ThH_3 by only 3.1 kcal/mol at 0 K. Thus, there is likely to be only a small fraction of ThH_5 present at 298 K.

Vibrational Frequencies. The calculated harmonic frequencies are given in Table 3. The calculated anharmonic ThH frequency is essentially the same as the experimental value in Ne.[10] The calculated harmonic ThH_2 asymmetric stretch frequency for the $^1A_1$ ground state is 17 cm^{-1} above the experimental Ne value.[10] This suggests that there is very little Ne matrix shift at this computational level if we assume a similar anharmonic effect to that in ThH. There is clearly a large Ar matrix effect on the symmetric stretch for ThH_2. The Th−H stretching frequencies in ThH_2^- are substantially smaller than in ThH_2 consistent, with the lengthening of the Th−H bond on the addition of the electron. The shifts from the neutral values in the $^2B_1$ state of the anion are significantly larger than for the $^2A_1$ state, even though the $^2B_1$ and $^2A_1$ states are essentially isoenergetic. The lengthening of the ThH bonds in ThH_2^- leads to a substantial reduction in the bending frequency due to a weakening of the interaction between the H atoms.

The three Th−H stretches in ThH_3 are very similar in magnitude to those in ThH_2. The three Th−H stretches in ThH_3^- are similar to those in the $^2A_1$ state of ThH_2^-. The calculated frequency for the triply degenerate asymmetric stretch in ThH_4 is 13 cm^{-1} above the experimental frequency[10] in Ne and 34 cm^{-1} above the experimental value in Ar, consistent with what was found for ThH and ThH_2. As expected, the addition of an electron to ThH_4 leads to a reduction in the Th−H stretch by about 200 cm^{-1}, consistent with the increase in the Th−H bond distance in the anion. The high energy vibrational transition in ThH_5 is for the H_2 moiety, which is almost 900 cm^{-1} below that in H_2 (ω_e = 4400 cm^{-1}) at the same level. The average of the Th−H stretches in the ThH_3 group of ThH_5 is about 10 cm^{-1} below the corresponding average in ThH_3. ThH_5^- has the highest Th−H stretch in all of the anions at 1446 cm^{-1}. The remaining Th−H stretches in ThH_5^- are consistent with the Th−H stretches in the other thorium hydride anions.

Adiabatic Electron Affinities. We first describe the calculated adiabatic EAs (AEAs) given in Table 4. The AEA(ThH_2) is 0.82 eV with a SO correction of 0.11 eV as compared to a SO correction of 0.07 eV for the AEA(ThH) at this computational level. As discussed above, the AEA(ThH) at this level is too low by 0.056 eV as compared to even higher level calculations.[8] The AEA(ThH_2) is 0.06 eV larger than the AEA(ThH) at this level. Much of this difference is due to the larger SO effect and ZPE difference for ThH_2. The AEA(ThH_3) is an additional 0.06 eV higher at 0.88 eV with a small SO correction of only 0.02 eV. The increase in the AEA is consistent with adding an electron to a Th atom, which has an increasing positive charge, although the effects are not very large, especially considering the ZPE effects. The AEA(ThH_4) decreases to 0.55 eV as one adds an electron to a closed shell molecule, forcing a distortion from the T_d geometry. ThH_4 can still add an electron due to the positive charge on the Th. The SO correction has now decreased to 0.01 eV. The SO

Table 3. Calculated Vibrational Frequencies (cm^{-1}) for $ThH_x^{0/-}$ (x = 1−5) at the CCSD(T) Level[a]

molecule	spin state	Th−H stretch	Th−H bend	expt.
ThH	$^2\Pi_{1/2}$	1547 ($\omega_e x_e$ = 20)		1511 (Ne), 1485 (Ar)
ThH	$2\Delta_{3/2}$	1550 ($\omega_e x_e$ = 19)		
ThH^-	$^3\Phi_2$	1306 ($\omega_e x_e$ = 19)		
ThH_2	$^1A_1$	1546 a_1	602 a_1	1480 (Ar)
		1493 b_2		1476(Ne), 1456(Ar)
ThH_2	$^3B_1$	1509 a_1	548 a_1	
		1478 b_2		
ThH_2^-	$^2B_1$	1282 a_1	397 a_1	
		1145 b_2		
ThH_2^-	$^2A_1$	1350 a_1	423 a_1	
		1258 b_2		
ThH_3	$^2A'$	1543 a_1	655 e	
		1467 e	177 a_1	
ThH_3^-	$^1A_1'$	1351 a_1	451 e′	
		1272 e′	411 a_2''	
ThH_4	$^1A_1$	1574 a_1	543 e	1456 (Ne), 1435 (Ar)
		1469 t_2	483 t_2	
ThH_4^{-b}	$^2A_1$	1366 a_1	448 e	
		1256 e	423 b_2	
		1245 b_2	235 e	
ThH_5^b	$^2A'$	3527 (H_2) á	1172 a′	
		1519 a′	856 a″	
		1483 a″	655 a′	
		1446 a′	524 a′	
			512 a″	
			401 a′	
			356 a′	
			348 a″	
$^1ThH_5^-$	$^1A_1$	1446 a_1	611 b_1	
		1279 e	553 e	
		1266 a_1	484 b_1	
		1219 b_2	331 b_2	
			348 e	

[a]All the frequencies were calculated with the awT-DK basis set unless noted. [b]The frequencies were calculated with the awD-DK basis set.

Table 4. Calculated CCSD(T) AEAs (eV) for $ThH_x^{0/-}$ (x = 1−5)

molecule	neutral state	anion state	CBS (awn-DK3)	ZPE (awT-DK)	SO (CASPT2)[a]	ΔH_{0K}
ThH	$^2\Pi$	$^3\Phi$	0.68	0.015	0.069	0.76
ThH_2	$^1A_1$	$^2B_1$	0.67	0.04	0.11	0.82
ThH_3	$^2A'$	$^1A_1'$	0.81	0.05	0.022	0.88
ThH_4	$^1A_1$	$^2A_1$	0.39	0.11[b]	0.014	0.51
ThH_5	$^2A'$	$^1A_1$	2.17	0.19[b]	0.004[c]	2.36

[a]SO-ADF (eV): 0.22 ThH_2, 0.017 ThH_3, and 0.001 ThH_4. [b]awD-DK. [c]SO-ADF (eV).

https://doi.org/10.1021/acs.jpca.2c01460
J. Phys. Chem. A 2022, 126, 2388−2396

correction for adding an electron to ThH_5 is essentially 0. ThH_5 has a higher AEA of 2.32 eV due to adding an electron to the molecule, which resembles a $ThH_3{\cdot}H_2$ complex. The resulting ThH_5^- structure is very stable, resulting in an AEA where the additional charge can be spread over the various H atoms and being stabilized by the +IV oxidation state of the Th.

Vertical Detachment Energies. The calculated first vertical electron detachment energies (VDEs) are given in Table 5 and compared to experiment where possible. The

Table 5. Calculated CCSD(T) First Vertical Electron Detachment Energies (VDE, eV) for $ThH_x^{0/-}$ (x = 1−5)

molecule	awD-DK	awT-DK	awQ-DK	CBS	CBS + SO	expt
ThH	0.56	0.65	0.69	0.71	0.78	0.87
ThH_2	0.61	0.69	0.72	0.73	0.84	0.871
ThH_3	0.78	0.83	0.85	0.86	0.88	0.88
ThH_4	0.77	0.77	0.79	0.80	0.81	
ThH_5	4.29	4.35	4.37	4.38	4.38	4.09

results for ThH have been discussed previously,[8] and a large number of states were predicted, resulting in a complex PES spectrum. A similar issue with a large number of states is predicted for ThH_2. As shown in Table 6, there are three

Table 6. Relative Energies (kcal/mol) of Low-Lying ThH_2^- and ThH_2 States at the CCSD(T)/CBS Limit and Geometry Parameters at the CCSD(T)/awQ-DK Level

state	ΔE_{0K} kcal/mol	r(Th−H) Å	∠H−Th−H°
	ThH_2^-		
$^2B_1$	0.0	2.120	130.9
$^2A_1$	0.03	2.121	130.8
$^2A_2$	3.4	2.104	120.5
$^2B_2$	10.7	2.109	131.8
$^4B_2$	13.0	2.136	102.8
$^4B_1$	17.6	2.107	80.1
$^4A_2$	20.2	2.120	116.7
$^4A_1$	20.9	2.114	82.8
$^4B_1$	23.4	2.092	81.3
	ThH_2		
$^1A_1$	0.0	2.033	124.9
$^3B_1$	6.6	2.063	117.1
$^1A_1$	7.8	1.992	64.7
$^3A_1$	8.0	2.067	121.7
$^3A_2$	13.1	2.044	87.6
$^3B_2$	26.7	2.078	99.4
$^3B_2$	34.3	2.102	104.8

different ThH_2^- states within 0.15 eV, with the two lowest energy states being essentially degenerate, which could complicate interpretation of the experimental spectra depending on the relaxation of the low-lying states in the molecular beam. There are an additional six states of the anion within 1 eV. For ThH_2 (Table 6), there are five states at the CCSD(T) level within 0.57 eV of each other.

In order to calculate the VDE spectrum for ThH_2^-, the first VDE from the lowest energy state of ThH_2^- to the ThH_2 state at the anion geometry is calculated at the CCSD(T)/CBS level with SO corrections. The remaining VDEs are then calculated from the relative energies obtained at the CASPT2/aQ-PP + SO level using the optimized ThH_2^- ($^2B_1$) CCSD(T)/awQ-DK geometry following our approach for ThH^-.[8] These results are given in Table 7. It is clear from the CASPT2-SO energy

Table 7. Calculated ThH_2 VDEs (eV) at the CASPT2/aQ-PP + SO Level Using the Optimized ThH_2^- ($^2B_1$) CCSD(T)/awQ-DK Geometry

state no.	VDE (eV)	assignment
1	0.84	95% $^1A_1$
2	0.96	47% $^3A_1$ + 48% $^3B_1$
3	1.00	49% $^3A_1$ + 48% $^3B_1$
4	1.13	92% $^3B_1$
5	1.14	95% $^3A_1$
6	1.37	49% $^3A_1$ + 49% $^3B_1$
7	1.37	49% $^3A_1$ + 49% $^3B_1$
8	1.66	98% $^3A_2$
9	1.68	97% $^3A_2$
10	1.69	94% $^3A_2$
11	1.86	95% $^1A_2$
12	1.95	43% $^1A_1$ + 24% $^3A_2$ + 20% $^3B_1$
13	2.07	61% $^3A_2$ + 28% $^3B_2$
14	2.11	87% $^1B_1$
15	2.12	26% $^1A_1$ + 37% $^3A_2$ + 33% $^3B_2$
16	2.17	58% $^3A_2$ + 40% $^3B_2$
17	2.19	11% $^1A_2$ + 63% $^3B_1$ + 23% $^3B_2$
18	2.29	50% $^1A_2$ + 47% $^3B_2$
19	2.31	41% $^3A_2$ + 59% $^3B_1$
20	2.33	19% $^1A_1$ + 26% $^3B_1$ + 50% $^3B_2$
21	2.34	91% $^3B_2$
22	2.37	50% $^3B_1$ + 43% $^3B_2$
23	2.37	29% $^3B_1$ + 69% $^3B_2$
24	2.42	38% $^1A_2$ + 53% $^3B_2$
25	2.51	35% $^3A_2$ + 61% $^3B_2$
26	2.53	31% $^3A_2$ + 60% $^3B_2$

levels that there are a large number of accessible excited states of ThH_2. For example, there are seven states within 0.55 eV of the lowest energy state at the CASPT2-SO level (up to 1.37 eV in the VDE). There are three states with VDEs near 1.7 eV, followed by two states within ±0.05 eV of 1.90 eV, and another grouping of three states near 2.10 eV. There are then 10 states between 2.15 and 2.5 eV. The large number of states is consistent with the complicated PES spectrum.

As with PES of ThH^-, it is very difficult to assign specific transitions in the experimental spectrum on the basis of the calculated values. However, we attempt to do so. We can assign the B peak (Figure 2 and Table 1) to the VDE at 1.00 eV and the C peak to the calculated VDE at 1.14 eV. The D peak is consistent with two calculated VDEs at 1.37 eV. The E peak could also be assigned to one of the two VDEs calculated at 1.37 eV. Peak F is consistent with the calculated VDE of 1.86 eV and possibly with the calculated VDE of 1.95 eV. Peak F is consistent with the two VDEs calculated at 2.11 and 2.12 eV. Obviously, there are many other VDEs that can be assigned to transitions in between the assigned peaks in PES (Figure 2).

There is excellent agreement with experiment[9] for PES of ThH_3^-, which is much simpler with an excited bound triplet state of the anion 0.39 eV higher in energy. There are no low-lying states in neutral ThH_3 to complicate PES. For ThH_4, there are no low-lying excited states in the neutral. The EA of

https://doi.org/10.1021/acs.jpca.2c01460
J. Phys. Chem. A 2022, 126, 2388−2396

Table 8. ThH_{x-1}-H BDEs (kcal/mol) and the Heats of Formation (kcal/mol) for ThH_x (x = 1−5)

reaction	CCSD(T)/CBS[a]	ZPE	ΔE_{SO}	$\Delta H(rxn)_{0K}$	molec	ΔH_f° (0 K)	ΔH_f° (298 K)
$ThH \rightarrow Th + H$	67.2	−2.4	−2.76	62.2	ThH	133.3	132.2
$ThH_2 \rightarrow ThH + H$	75.0	−3.0	−4.88	67.1	ThH_2	117.7	116.7
$ThH_3 \rightarrow ThH_2 + H$	72.7	−3.3	−0.03	69.4	ThH_3	100.0	98.4
$ThH_4 \rightarrow ThH_3 + H$	79.5	−3.9	−1.0	74.6	ThH_4	77.1	74.5
$ThH_5 \rightarrow ThH_4 + H$	36.5	−5.8		30.7	ThH_5	98.0	94.9

[a]awn-DK basis sets.

Table 9. Hydride Affinities (kcal/mol) for ThH_x (x = 0−4) and the Heats of Formation (kcal/mol) for ThH_x^- (x = 1−5)

reaction	CBS (awn-DK)	ZPE	ΔE_{SO}	$\Delta H(rxn)_{0K}$	molec	ΔH_f° (0 K)	ΔH_f° (298 K)
$Th + H^- \rightarrow ThH^-$	−66.2	1.9	0.54	−63.8	ThH^-	114.3	113.3
$ThH + H^- \rightarrow ThH_2^-$	−73.1	2.0	0.75	−70.4	ThH_2^-	97.2	96.2
$ThH_2 + H^- \rightarrow ThH_3^-$	−74.2	2.2	3.87	−68.1	ThH_3^-	63.3	61.6
$ThH_3 + H^- \rightarrow ThH_4^-$	−71.1	1.3	1.15	−68.6	ThH_4^-	29.0	26.9
$ThH_4 + H^- \rightarrow ThH_5^-$	−69.3	1.5	0	−67.8	ThH_5^-	−4.6	−7.6

Table 10. NBO/HF Charges (q) and Th Population at the aD-DK Level

ThHx	state	qTh	qH	5f (5fα/5fβ)	6d (6dα/6dβ)	7s (7sα/7sβ)	7p(7pα/7pβ)	H 1s (1sα/1sβ)
ThH	$^2\Pi_{1/2}$	0.585	−0.585	0.08 (0.06/0.02)	1.50(1.22/0.28)	1.81(0.90/0.90)	0.04(0.03/0.01)	1.57(0.78/0.78)
ThH	$^2\Delta_{3/2}$	0.598	−0.598	0.04(0.02/0.02)	1.48(1.24/0.24)	1.86(0.93/0.93)	0.04(0.02/0.02)	1.58(0.79/0.79)
ThH^-	$^3\Phi_2$	−0.297	−0.703	0.03(0.02/0.01)	2.22(2.04/0.18)	1.87(0.94/0.94)	0.18(0.15/0.03)	1.67(0.84/0.84)
ThH^-	$^3\Sigma_0^-$	−0.305	−0.695	0.04(0.02/0.01)	2.24(2.04/0.20)	1.86(0.93/0.93)	0.18(0.16/0.02)	1.67(0.83/0.83)
ThH_2	$^1A_1$	1.169	−0.585	0.08	1.10	1.61	0.05	1.57
ThH_2	$^3B_1$	1.234	−0.617	0.08(0.05/0.03)	1.73(1.47/0.26)	0.85(0.74/0.11)	0.13(0.12/0.01)	1.60(0.80/0.80)
ThH_2^-	$^2B_1$	0.297	−0.649	0.07(0.04/0.03)	0.98(0.53/0.45)	1.67(0.83/0.83)	0.99(0.95/0.04)	1.62(0.81/0.81)
ThH_2^-	$^2A_1$	0.337	−0.669	0.11(0.08/0.03)	1.14(0.71/0.43)	1.64(0.82/0.82)	0.74(0.68/0.06)	1.64(0.82/0.81)
ThH_3	$^2A'$	1.804	−0.601	0.10(0.05/0.05)	1.37(0.96/0.41)	0.69(0.53/0.16)	0.06(0.05/0.01)	1.58(0.79/0.79)
ThH_3^-	$^1A_1'$	0.912	−0.637	0.09	1.64	1.33		1.62
ThH_4	$^1A_1$	2.325	−0.581	0.12	1.17	0.42		1.57
ThH_4^-	$^2A_1$	1.629	−0.657	0.09(0.05/0.04)	1.73(1.27/0.46)	0.01(0.01/0.0)	0.01(0.01/0.01)	1.65(0.82/0.82)
ThH_5	$^2A'$	1.759	−0.576(x2)	0.13(0.08/0.05)	1.53(1.05/0.48)	0.56(0.41/0.15)	0.05(0.04/0.01)	1.56(0.78/0.78)
			−0.554					1.53(0.78/0.77)
			−0.057					1.04(0.54/0.50)
			0.005					0.99(0.52/0.47)
ThH_5^-	$^1A_1$	2.154	−0.624(x4)	0.15	1.28	0.44		1.62
			−0.659					1.65

ThH_5 has been previously discussed, and there is about a 2 eV difference between the adiabatic and vertical values.

Thermochemistry. In order to calculate the heats of the formation of these neutral and anionic ThH_x species, for x = 2−5, we build up the bond energies sequentially from ThH, where we have a reliable previous heat of formation prediction at an even higher computational level.[8] The Th−H bond dissociation energies (BDEs) for various compounds calculated at the FPD level are given in Table 8. The values for ThH were obtained using the known atomic heats of the formation of $\Delta H_{f,0K}$ (Th) = 143.9 ± 1.4 kcal/mol[51] and $\Delta H_{f,0K}$ (H) = 51.63 kcal/mol from the active thermochemical tables.[52−54] The values for ThH are ΔH_f° (0 K) = 133.3 and ΔHf° (298 K) = 132.2 kcal/mol.

The Th−H BDEs increased from 62 to 76 kcal/mol from ThH to ThH_4. The average Th−H BDE for ThH_4 is 69 kcal/mol, much less than the average C−H BDE in CH_4. This is in contrast to the fluorides, where the average Th−F BDE in ThF_4 is substantially larger than the average C−F BDE in CF_4.[55] There is a significant decrease in the Th−H BDE going from ThH_4 to ThH_5 due to the weak complex, that is, ThH_5. The bond energies can then be used to calculate the heat of the formation of the hydrides. There is a significant SO contribution to the bond energy of ThH and an even larger one for ThH_2 of almost −5.0 kcal/mol. The SO correction for the Th−H BDE in ThH_3 is negligible and changes to −1.0 kcal/mol for ThH_4.

The hydride affinities for the thorium hydrides excluding Th are remarkably similar, falling in the range of 67−71 kcal/mol and are essentially independent of the number of H atoms on the Th (Table 9). There is a significant SO correction for the hydride affinity of ThH_2, but the remaining SO corrections are on the order of 1 kcal/mol or less.

Electronic Structure Analysis. The NBO analysis (Table 10) provides useful insights into how the electronic charge is distributed. Th−H has about 0.6e on the Th, showing significant ionic character. For ThH, the bonding in the ground state comes from a combination of the $7s^26d^2$ state of Th bonding with the 1s electron of H and the $7s^26d^1$ state of Th^+ with the closed-shell $1s^2$ state of H^-. For ThH^-, the bonding is best considered by adding H^- to Th, as the Th EA is lower than that of H. The addition of the electron to Th−H

https://doi.org/10.1021/acs.jpca.2c01460
J. Phys. Chem. A 2022, 126, 2388−2396

to form the anion leads to most of the additional negative charge being added to the Th, almost 0.9*e* on the Th with only 0.1*e* being delocalized onto the already quite negative H. The Th 7s and H 1s orbitals are doubly occupied with two electrons on the Th occupying 6d orbitals.

For ThH_2, there is approximately a +1.2 charge on the Th. When ThH_2^- is generated by the addition of an electron, 0.9e of that electron goes onto the Th just as in ThH^-. ThH_3 has a charge of +1.80 on the Th, so that there is about 0.6*e* on each H. Thus, the ionicity of the Th−H bond is approximately constant for the first three H atoms that are added. The addition of an electron to ThH_3 leads again to about 0.9*e* of the additional electron localizing on the Th. This is consistent with the negative charge already on the H ligands; thus, the H ligands do not want to accept an additional charge. For ThH_4, the Th−H bonds are only slightly less ionic than in the thorium hydrides with one to three hydrogens. The addition of the electron now starts to delocalize onto the hydrogens as there is only an additional ∼0.7*e* on the Th. The charge on Th in ThH_5, which is a complex of ThH_3 and H_2, is similar to that in ThH_3. The addition of the electron makes the Th more positive in ThH_5^- than in ThH_5 due to the different structures.

The analysis of the valence orbital contributions to the bonding shows that the Th behaves more like a transition metal with a little 5f character, with 0.0−0.15 electrons in the 5f. Most of the valence population on Th is in the 7s and 6d. The electron configuration of the Th in ThH is predominantly $7s^{1.8}6d^{1.5}$ and that of ThH^- is $7s^{1.9}6d^{2.2}7p^{0.2}$. The 7s electrons are doubly occupied. The ground state of ThH_2 has an electron configuration of $7s^{1.6}6d^1$. The addition of the electron leads to two low-lying states. In both cases, the extra electron goes mostly into the 7p with an electron configuration of $7s^{1.7}6d^{1.0}7p^{1.0}$ for the $^2B_1$ state of ThH_2^-. Note that ThH_2^- is the only species with a significant 7p population. Again, the 7s is doubly occupied. For ThH_3, there is still a significant 6d character but there is a loss of electron density in the 7s as expected for the formal Th(III) oxidation state with the Th having a $7s^{0.7}6d^{1.4}$ electron configuration. The 7s orbital is no longer doubly occupied, and there is unpaired spin in both the 7s and 6d. The addition of an electron to ThH_3 to generate closed-shell ThH_3^- is predominantly to the 7s, with some going into the 6d as well, for a Th electron configuration of $7s^{1.3}6d^{1.6}$. For closed-shell ThH_4, there is even less 7s electron density with a Th electron configuration of $7s^{0.4}6d^{1.2}$. The addition of the electron to ThH_4 leads to a dramatic change with essentially all of the 7s density lost and a significant increase in the 6d population, giving a $6d^{1.7}$ electron configuration. The electron configuration of $7s^{0.6}6d^{1.5}$ for the Th in ThH_5 is similar to ThH_3 as expected due to its structure as a complex of ThH_3 with H_2. In ThH_5^- the Th electron configuration is $7s^{0.4}6d^{1.3}$.

The ground state electron configurations of Th, Th(I), Th(II), and Th(III) are $7s^26d^2$, $7s^16d^2$, $5f^16d^1$, and $5f^1$, respectively.[38,56] There is a low-lying $7s^26d^1$ excited state for Th(I) that is 0.23 eV above the ground state and a low-lying $6d^2$ excited state that is 0.008 eV above the ground state for Th(II). The population results above show that the addition of the H ligands is clearly dominated by bonding to 7s and 6d electrons and that 5f electrons play only a minimal role, if any, in the bonding. The bonding in ThH to ThH_4 has a significant ionic component but the bonds are not fully ionic as shown by the H 1s populations and the electron configurations in Th. The Th electron configurations in the hydrides are usually not dominated by the ground state configuration of the corresponding ionic Th species in the highest formal oxidation state.

CONCLUSIONS

The current work continues our study[8] of the interactions of hydrogen with Th for up to five hydrogen atoms using a combination of high-level electronic structure calculations and PES experiments on ThH_2^-. As found for ThH^-, there are many low-lying transitions in ThH_2, as observed in the photodetachment spectrum of ThH_2^-. There are a significant number of low-lying states in both ThH_2 and ThH_2^- and SO calculations on ThH_2 are needed to predict the transitions in the ThH_2^- photodetachment spectrum. At the CCSD(T)/CBS level, the ground state of ThH_2^- is the $^2B_1$, with the $^2A_1$ state only 0.03 eV higher in energy. At the CASPT2 level, the ground state is a mixture of 50% $^2A_1$ + 43% $^2B_1$ + 6% $^2A_2$. The first excited state at the CASPT2 level is 0.29 eV higher in energy and is a mixture of 43% $^2A_1$ + 30% $^2B_1$ + 23% $^2A_2$. The ground state for ThH_2 is $^1A_1$, with the $^3B_1$ state 0.29 eV higher in energy at the CCSD(T)/CBS level. At the CASPT2 level, the ground state is $^1A_1$ with the first excited state a mixture of 47% $^3A_1$ + 48% $^3B_1$ 0.12 eV higher in energy and a second excited state 0.16 eV higher in energy than the ground state, that is, a mixture of 49% $^3A_1$ + 48% $^3B_1$.

The states for ThH_3 and ThH_3^- are simpler to describe, with the former being a near planar $^2A_1$ state in C_{3v} symmetry and the latter being a planar $^1A_1'$ state in D_{3h} symmetry. The first excited state at the CCSD(T)/CBS level for ThH_3^- is the $^3A''$, which is 0.39 eV higher in energy. The CASPT2 energy for this state is 0.41 eV, showing only a minor SO effect. At the CASPT2 level, the first excited state of ThH_3 is 0.84 eV higher in energy. ThH_4 is clearly a ground state singlet in T_d symmetry. At the CASPT2 level, the first excited state of ThH_4^- is 0.53 kcal/mol higher in energy.

The AEA for ThH_2 is calculated to be 0.82 eV at the FPD level used in the current work, with a SO correction of 0.11 eV. The calculated VDE for ThH_2^- differs by only 0.03 eV from the experimental value of 0.871 eV. For ThH_2^-, the calculated AEA and VDE differ by only 0.02 eV, very similar to the differences for these values for ThH^-. The VDE and AEA are essentially the same for ThH_3 and are in excellent agreement with experiment. The SO correction for the ThH_3 is much smaller, 0.022 eV, than for ThH_2. There is a larger difference between the AEA and VDE for ThH_4 due to the larger change in geometry as the ThH_4 tetrahedron distorts on binding an electron. Because of the structural stability of ThH_4, the AEA drops by 0.37 eV from that of ThH_3. Note that for ThH to ThH_4, the AEA and VDE values are all less than 1.0 eV. ThH_5^-, as noted previously,[9] is quite stable and has a C_{4v} structure rather than the D_{3h} structure of ThF_5^-.[50] ThH_5 is best described as a complex of H_2 bonded to ThH_3, so the VDE and AEA differ by 1.73 eV.

The Th−H BDEs increase from ThH (62 kcal/mol) to ThH_4 (75 kcal/mol). The Th−H BDE for $ThH_5 \rightarrow ThH_4 + H$ is much smaller due to the dramatic change in geometry and the stability of ThH_4. The hydride affinities are comparable for ThH_2 to ThH_4, approximately 70 kcal/mol. The hydride affinity for ThH is slightly smaller at 64 kcal/mol. The increase in the Th−H BDEs from ThH to ThH_4 is consistent with the increase in positive charge from 0.60 for ThH to 2.32 for ThH_4. The charge also becomes more positive in the anions from −0.30 eV for ThH^- to 2.15 in ThH_5^-.

https://doi.org/10.1021/acs.jpca.2c01460
J. Phys. Chem. A 2022, 126, 2388−2396

The population analysis shows the importance of the 7s and 6d Th orbitals in the bonding of these species, which have a significant ionic bonding component. Again, the results show that the hydrogen ligand provides an interesting probe into the electron configurations of the actinide in an actinide hydride.

■ ASSOCIATED CONTENT

Supporting Information

The Supporting Information is available free of charge at https://pubs.acs.org/doi/10.1021/acs.jpca.2c01460.

Complete citations for refs 31 and 32 and total energy contributions using different basis sets (PDF)

■ AUTHOR INFORMATION

Corresponding Authors

Kit H. Bowen − *Department of Chemistry, Johns Hopkins University, Baltimore, Maryland 21218, United States;* orcid.org/0000-0002-2858-6352; Email: kbowen@jhu.edu

David A. Dixon − *Department of Chemistry and Biochemistry, University of Alabama, Tuscaloosa, Alabama 35401, United States;* orcid.org/0000-0002-9492-0056; Email: dadixon@ua.edu

Authors

Monica Vasiliu − *Department of Chemistry and Biochemistry, University of Alabama, Tuscaloosa, Alabama 35401, United States*

Mary Marshall − *Department of Chemistry, Johns Hopkins University, Baltimore, Maryland 21218, United States*

Zhaoguo Zhu − *Department of Chemistry, Johns Hopkins University, Baltimore, Maryland 21218, United States;* orcid.org/0000-0002-4395-9102

Complete contact information is available at: https://pubs.acs.org/10.1021/acs.jpca.2c01460

Notes

The authors declare no competing financial interest.

■ ACKNOWLEDGMENTS

This work was supported by the U.S. Department of Energy, Office of Science, Office of Basic Energy Sciences, Heavy Element Chemistry program at Johns Hopkins University (K.H.B., experiment) through the grant number DE-SC0019317 and at the University of Alabama (D.A.D., computational) through grant no. DE-SC0018921. D.A.D. thanks the Robert Ramsay Fund at the University of Alabama.

■ REFERENCES

(1) Tang, R.; Si, R.; Fei, Z.; Fu, X.; Brage, T.; Liu, H.; Chen, C.; Ning, C. Candidate for Laser Cooling of a Negative Ion: High-Resolution Photoelectron Imaging of Th^-. *Phys. Rev. Lett.* **2019**, *123*, 203002-1−203002-6.

(2) Zhu, Z.; Marshall, M.; Harris, R. M.; Bowen, K. H.; Vasiliu, M.; Dixon, D. A. The Th_2O^-, Th_2Au^- and $Th_2AuO_{1,2}^-$ Anions: Photoelectron Spectroscopic and Computational Characterization of Energetics and Bonding. *J. Phys. Chem. A* **2021**, *125*, 258−271.

(3) Ciborowski, S. M.; Liu, G.; Blankenhorn, M.; Harris, R. M.; Marshall, M. A.; Zhu, Z.; Bowen, K. H.; Peterson, K. A. The Electron Affinity of the Uranium Atom. *J. Chem. Phys.* **2021**, *154*, 224307-1−224307-8.

(4) Dixon, D. A.; Feller, D.; Peterson, K. A. A Practical Guide to Reliable First Principles Computational Thermochemistry Predictions Across the Periodic Table. In *Annual Reports in Computational Chemistry*; Wheeler, R. A.; Section, E. d.; Tschumper, G. S., Eds.; Elsevier: Amsterdam, 2012; Chapter 1, Vol. *8*, pp 1−28.

(5) Feller, D.; Peterson, K. A.; Dixon, D. A. Further Benchmarks of a Composite, Convergent, Statistically-Calibrated Coupled Cluster-Based Approach for Thermochemical and Spectroscopic Studies. *Mol. Phys.* **2012**, *110*, 2381−2399.

(6) Peterson, K. A.; Feller, D.; Dixon, D. A. Chemical Accuracy in Ab Initio Thermochemistry and Spectroscopy: Current Strategies and Future Challenges. *Theor. Chem. Acc.* **2012**, *131*, 1079-1−1079-20.

(7) Feller, D.; Peterson, K. A.; Dixon, D. A. The Impact of Larger Basis Sets and Explicitly Correlated Coupled Cluster Theory on the Feller-Peterson-Dixon Composite Method. In *Annual Reports in Computational Chemistry*; Dixon, D. A., Ed.; Elsevier: Amsterdam, 2016; Vol. *12*, pp 47−78.

(8) Vasiliu, M.; Peterson, K. A.; Marshall, M.; Zhu, Z.; Tufekci, B. A.; Bowen, K. H.; Dixon, D. A. The Interaction of Th with $H^{0/-/+}$. Combined Experimental and Theoretical Thermodynamic Properties. *J. Phys. Chem. A* **2022**, *126*, 198−210.

(9) Marshall, M.; Zhu, Z.; Harris, R.; Bowen, K. H.; Wang, W.; Wang, J.; Gong, C.; Zhang, X. ThH_5: An Actinide-Containing Superhalogen Molecule. *ChemPhysChem* **2021**, *22*, 5−8.

(10) Wang, X.; Andrews, L.; Gagliardi, L. Infrared Spectra of ThH_2, ThH_4, and the Hydride Bridging $ThH_4(H_2)_x$ (x = 1-4) Complexes in Solid Neon and Hydrogen. *J. Phys. Chem. A* **2008**, *112*, 1754−1761.

(11) Grant, D. J.; Stewart, T. J.; Bau, R.; Miller, K. A.; Mason, S. A.; Gutmann, M.; McIntyre, G. J.; Gagliardi, L.; Evans, W. J. Uranium and Thorium Hydride Complexes as Multielectron Reductants: A Combined Neutron Diffraction and Quantum Chemical Study. *Inorg. Chem.* **2012**, *51*, 3613−3624.

(12) Gerhards, M.; Thomas, O. C.; Nilles, J. M.; Zheng, W.-J.; Bowen, K. H. Cobalt-Benzene Cluster Anions: Mass Spectrometry and Negative Ion Photoelectron Spectroscopy. *J. Chem. Phys.* **2002**, *116*, 10247−10252.

(13) Ho, J.; Ervin, K. M.; Lineberger, W. C. Photoelectron spectroscopy of metal cluster anions: Cu_n^-, Ag_n^-, and Au_n^-. *J. Chem. Phys.* **1990**, *93*, 6987−7002.

(14) Purvis, G. D., III; Bartlett, R. J. A Full Coupled-Cluster Singles and Doubles Model: The Inclusion of Disconnected Triples. *J. Chem. Phys.* **1982**, *76*, 1910−1918.

(15) Raghavachari, K.; Trucks, G. W.; Pople, J. A.; Head-Gordon, M. A Fifth-order Perturbation Comparison of Electron Correlation Theories. *Chem. Phys. Lett.* **1989**, *157*, 479−483.

(16) Watts, J. D.; Gauss, J.; Bartlett, R. J. Coupled-Cluster Methods with Non-iterative Triple Excitations for Restricted Open-Shell Hartree-Fock and Other General Single-Determinant Reference Functions. Energies and Analytical Gradients. *J. Chem. Phys.* **1993**, *98*, 8718−8733.

(17) Bartlett, R. J.; Musiał, M. Coupled-Cluster Theory in Quantum Chemistry. *Rev. Mod. Phys.* **2007**, *79*, 291−352.

(18) Douglas, M.; Kroll, N. M. Quantum Electrodynamical Corrections to the Fine Structure of Helium. *Ann. Phys.* **1974**, *82*, 89−155.

(19) Jansen, G.; Hess, B. A. Revision of the Douglas-Kroll Transformation. *Phys. Rev. A* **1989**, *39*, 6016−6017.

(20) Wolf, A.; Reiher, M.; Hess, B. A. The Generalized Douglas-Kroll Transformation. *J. Chem. Phys.* **2002**, *117*, 9215−9226.

(21) Kendall, R. A.; Dunning, T. H., Jr.; Harrison, R. J. Electron Affinities of the First-Row Atoms Revisited. Systematic Basis Sets and Wave Functions. *J. Chem. Phys.* **1992**, *96*, 6796−6806.

(22) De Jong, W. A.; Harrison, R. J.; Dixon, D. A. Parallel Douglas−Kroll Energy and Gradients in NWChem: Estimating Scalar Relativistic Effects Using Douglas−Kroll Contracted Basis Sets. *J. Chem. Phys.* **2001**, *114*, 48−53.

(23) Peterson, K. A. Correlation Consistent Basis Sets for Actinides. I. The Th and U Atoms. *J. Chem. Phys.* **2015**, *142*, 074105.

(24) Feng, R.; Peterson, K. A. Correlation consistent basis sets for actinides. II. The atoms Ac and Np−Lr. *J. Chem. Phys.* **2017**, *147*, 084108−084112.

(25) Peterson, K. A.; Woon, D. E.; Dunning, T. H., Jr. Benchmark Calculations with Correlated Molecular Wave Function. IV. The Classical Barrier Height of the H+H_2→H_2+H Reaction. *J. Chem. Phys.* **1994**, *100*, 7410−7415.
(26) Feller, D.; Peterson, K. A.; Hill, J. G. On the Effectiveness of CCSD(T) Complete Basis Set Extrapolations for Atomization Energies. *J. Chem. Phys.* **2011**, *135*, 044102.
(27) Watts, J. D.; Gauss, J.; Bartlett, R. J. Coupled-Cluster Methods with Non-iterative Triple Excitations for Restricted Open-Shell Hartree-Fock and Other General Single-Determinant Reference Functions. Energies and Analytical Gradients. *J. Chem. Phys.* **1993**, *98*, 8718−8733.
(28) Deegan, M. J. O.; Knowles, P. J. Perturbative Corrections to Account for Triple Excitations in Closed and Open Shell Coupled Cluster Theories. *Chem. Phys. Lett.* **1994**, *227*, 321−326.
(29) Rittby, M.; Bartlett, R. J. An Open-Shell Spin-Restricted Coupled Cluster Method: Application to Ionization Potentials in N_2. *J. Phys. Chem.* **1988**, *92*, 3033−3036.
(30) Knowles, P. J.; Hampel, C.; Werner, H. J. Coupled Cluster Theory for High Spin, Open Shell Reference Wave Functions. *J. Chem. Phys.* **1993**, *99*, 5219−5227.
(31) Werner, H.-J.; Knowles, P. J.; Knizia, G., Manby, F. R.; Schütz, M.; Celani, P.; Györffy, W.; Kats, D.; Korona, T.; Lindh, R.; et al. MOLPRO, version 2019.2, A Package of Ab Initio Programs. https://www.molpro.net (accessed Jan 1, 2021).
(32) Werner, H.-J.; Knowles, P. J.; Manby, F. R.; Black, J. A.; Doll, K.; Heßelmann, A.; Kats, D.; Köhn, A.; Korona, T.; Kreplin, D. A.; et al. The Molpro Quantum Chemistry Package. *J. Chem. Phys.* **2020**, *152*, 144107-1−144107-24.
(33) Roos, B. O.; Taylor, P. R.; Sigbahn, P. E. M. A Complete Active Space SCF Method (CASSCF) Using a Density-matrix Formulated Super-CI Approach. *Chem. Phys.* **1980**, *48*, 157−173.
(34) Siegbahn, P. E. M.; Almlöf, J.; Heiberg, A.; Roos, B. O. The Complete Active Space SCF (CASSCF) Method in a Newton-Raphson Formulation with Application to the HNO Molecule. *J. Chem. Phys.* **1981**, *74*, 2384−2396.
(35) Dunning, T. H., Jr. Gaussian Basis Set for Use in Correlated Molecular Calculations. I. The Atoms Boron through Neon and Hydrogen. *J. Chem. Phys.* **1989**, *90*, 1007−1023.
(36) Kendall, R. A.; Dunning, T. H., Jr.; Harrison, R. J. Electron Affinities of the First-Row Atoms Revisited. Systematic Basis Sets and Wave Functions. *J. Chem. Phys.* **1992**, *96*, 6796−6806.
(37) Weigand, A.; Cao, X.; Hangele, T.; Dolg, M. Relativistic Small-Core Pseudopotentials for Actinium, Thorium, and Protactinium. *J. Phys. Chem. A* **2014**, *118*, 2519−2530.
(38) Kramida, A.; Ralchenko, Yu.; Reader, J. and NIST ASD Team. (2020). NIST Atomic Spectra Database (ver. 5.8), [Online]. Available; National Institute of Standards and Technology: Gaithersburg, MD. 2020, https://physics.nist.gov/asd (accessed July 7, 2021).
(39) VanGundy, R. A.; Bartlett, J. H.; Heaven, M. C.; Battey, S. R.; Peterson, K. A. Spectroscopic and Theoretical Studies of ThCl and $ThCl^+$. *J. Chem. Phys.* **2017**, *146*, 054307.
(40) Barker, B. J.; Antonov, I. O.; Heaven, M. C.; Peterson, K. A. Spectroscopic Investigations of ThF and ThF^+. *J. Chem. Phys.* **2012**, *136*, 104305-1−104305-9.
(41) Nguyen, D.-T.; Steimle, T.; Linton, C.; Cheng, L. Optical Stark and Zeeman Spectroscopy of Thorium Fluoride (ThF) and Thorium Chloride (ThCl). *J. Phys. Chem. A* **2019**, *123*, 1423−1433.
(42) Andersson, K.; Malmqvist, P. A.; Roos, B. O.; Sadlej, A. J.; Wolinski, K. Second-Order Perturbation Theory with a CASSCF Reference Function. *J. Phys. Chem.* **1990**, *94*, 5483−5488.
(43) Andersson, K.; Malmqvist, P. Å.; Roos, B. O. Second-Order Perturbation Theory with a Complete Active Space Self-Consistent Field Reference Function. *J. Chem. Phys.* **1992**, *96*, 1218−1226.
(44) Ghigo, G.; Roos, B. O.; Malmqvist, P.-Å. A Modified Definition of the Zeroth-Order Hamiltonian in Multiconfigurational Perturbation Theory (CASPT2). *Chem. Phys. Lett.* **2004**, *396*, 142−149.
(45) Berning, A.; Schweizer, M.; Werner, H.-J.; Knowles, P. J.; Palmieri, P. Spin-Orbit Matrix Elements for Internally Contracted Multireference Configuration Interaction Wavefunctions. *Mol. Phys.* **2000**, *98*, 1823−1833.
(46) Reed, A. E.; Curtiss, L. A.; Weinhold, F. Intermolecular Interactions from a Natural Bond Orbital, Donor-Acceptor Viewpoint. *Chem. Rev.* **1988**, *88*, 899−926.
(47) Weinhold, F.; Landis, C. R. *Valency and Bonding: A Natural Bond Orbital Donor-Acceptor Perspective*; University Press: Cambridge, U.K., 2005.
(48) Glendening, E. D.; Badenhoop, J. K.; Reed, A. E.; Carpenter, J. E.; Bohmann, J. A.; Morales, C. M.; Karafiloglou, P.; Landis, C. R.; Weinhold, F. *Natural Bond Order 7.0*; Theoretical Chemistry Institute, University of Wisconsin: Madison, WI, 2018.
(49) Glendening, E. D.; Landis, C. R.; Weinhold, F. NBO 7.0: New Vistas in Localized and Delocalized Chemical Bonding Theory. *J. Comput. Chem.* **2019**, *40*, 2234−2241.
(50) Andrews, L.; Thanthiriwatte, K. S.; Wang, X.; Dixon, D. A. Thorium Fluorides ThF, ThF_2, ThF_3, ThF_4, $ThF_3(F_2)$ and ThF_5^- Characterized by Infrared Spectra in Solid Argon and Electronic Structure and Vibrational Frequency Calculations. *Inorg. Chem.* **2013**, *52*, 8228−8233.
(51) Cox, J. D.; Wagman, D. D.; Medvedev, V. A. *CODATA Key Values for Thermodynamics*; Hemisphere Publishing Corp.: New York, 1989.
(52) https://atct.anl.gov/Thermochemical%20Data/version%201.122g/index.php (accessed Jan 18, 2019).
(53) Ruscic, B.; Pinzon, R. E.; Morton, M. L.; von Laszevski, G.; Bittner, S. J.; Nijsure, S. G.; Amin, K. A.; Minkoff, M.; Wagner, A. F. Introduction to Active Thermochemical Tables: Several "Key" Enthalpies of Formation Revisited. *J. Phys. Chem. A* **2004**, *108*, 9979−9997.
(54) Changala, P. B.; Nguyen, T. L.; Baraban, J. H.; Ellison, G. B.; Stanton, J. F.; Bross, D. H.; Ruscic, B. Active Thermochemical Tables: The Adiabatic Ionization Energy of Hydrogen Peroxide. *J. Phys. Chem. A* **2017**, *121*, 8799−8806.
(55) Vasiliu, M.; Battey, S. R.; Lu, Q.; Peterson, K. A.; Andrews, L.; Dixon, D. A. Gas Phase Properties of MX_2 and MX_4 (X=F, Cl) for M = Group 4, Group 14, Ce, and Th. K. S. Thanthiriwatte. *J. Phys. Chem. A* **2015**, *119*, 5790−5803.
(56) Wickleder, M. S.; Fourest, B.; Dorhout, P. K. Thorium. In *The Chemistry of the Actinide and Transactinide Elements*, 3rd ed.; Morss, L. R.; Edelstein, N. M.; Fuger, J., Eds.; Springer: Dordrecht, NL, 2006; Vol. *1*, pp 52−160.

https://doi.org/10.1021/acs.jpca.2c01460
J. Phys. Chem. A 2022, 126, 2388−2396